Inspection of baked carbon anodes using acoustic techniques

Moez Ben Boubaker[1], Donald Picard[2], Jayson Tessier[3], Houshang Alamdari[4], Mario Fafard[5], Carl Duchesne[6]

[1]PhD student, Aluminum Research Centre – REGAL, Département de génie chimique, Université Laval
[2]Research Assistant, Aluminum Research Centre – REGAL, Département de génie civil, Université Laval
[3]Manager, Pilot Zone Operations, Alcoa Primary Metals Smelting Center of Excellence
[4]Professor, Aluminum Research Centre – REGAL, Département de génie des mines, de la métallurgie et des matériaux, Université Laval
[5]Professor, Aluminum Research Centre – REGAL, Département de génie civil, Université Laval
[6]Professor, Aluminum Research Centre – REGAL, Département de génie chimique, Université Laval
Corresponding author: carl.duchesne@gch.ulaval.ca

Keywords: Baked carbon anode; Non-destructive testing; Acoustics; PCA; Aluminum smelting

Abstract

High quality baked carbon anodes contribute to optimal performance of aluminum reduction cells. However, the currently decreasing quality and increasing variability of anode raw materials (coke and pitch) make it challenging to manufacture anodes with consistent overall quality. Intercepting faulty anodes (i.e. damaged due to internal cracks and voids) before they are set in reduction cells and deteriorate their performance is therefore important. However, this is a difficult task even in modern and well instrumented anode plants because lab testing using core samples can only characterize a small proportion of the anode production due to the costly, time consuming, and destructive nature of the analytical methods, and these results are not necessarily representative of the whole anode block. Therefore, the objective of this work is to develop a rapid and non-destructive method for quality control of baked anodes, based on acoustic techniques. The acoustic response of the anodes was analyzed using a combination of signal processing and multivariate statistical methods. The sensitivity of the acoustic signals to various defects is demonstrated using a sliced anode which was submitted to CT-scan (X-ray) to visualize the internal structure.

1. Introduction

The currently decreasing quality and increasing variability of anode raw materials (coke and pitch) make it challenging to manufacture anodes with consistent overall quality. Intercepting faulty anodes before they are set in reduction cells and deteriorate their performance (i.e. energy consumption and efficiency) requires testing all or the majority of manufactured anodes. However, even in modern and well instrumented anode manufacturing plants, the traditional lab inspection strategy based on core sampling can at best evaluate the properties of about 1% of the manufactured anodes due to the costly, time consuming, and destructive nature of the analytical methods. In addition, core sample properties are typically available after the anode was set in the reduction cells due to the long lab delays. For economical and logistics reasons, it is generally not possible to improve the rate of anode testing by increasing the lab work load. Furthermore, the properties obtained from core samples are not necessarily representative of the whole anode block as reported by Sinclair and Sadler [1-2], who provide a complete list of issues related with the use of core samples for quality control and decision making. Indeed, anode blocks are heterogeneous materials that may contain different types of internal defects (i.e. coke particles not penetrated by pitch, regions of high/low pitch concentration, pores and cracks) which can lead to anisotropic distribution of properties within the block. The current strategy may completely miss these defects if the core is not sampled where the defects are located. Hence, the mechanical properties, electrical resistivity obtained from core samples may only reflect localized properties. Therefore, rapid and non-destructive techniques to inspect anode blocks should be investigated in order to

provide a better picture of the block quality in a timely fashion. This would allow anode sorting strategies to be put in place and feedback corrective adjustments to be implemented on paste plant and baking furnace operation parameters.

Acoustic emission (AE) methods have been widely used as a non-destructive technique in the inspection of composite materials, such as concrete and refractories [3-5]. However, applications of AE for testing complex porous materials naturally containing pores and cracks, such as baked carbon anodes, are not as common as for denser materials such as parts made of metal alloys or highly graphitized carbon materials, which are expected to be free of internal voids. The main issue with anodes is to separate defects affecting their performance in the reduction cells from the internal porosity which is always present when both types of voids attenuate the acoustic waves propagating through the materials. The only publicly available reports on the application of acoustic methods on carbon electrodes appears to be those of Allaire [6] and Allaire et al. [7] using the SonicByte^{TM} system [8]. Their work mainly focused on measuring the elastic properties of refractory and carbonaceous materials as a mean of detecting defects. Although, this technique may help identify faulty anodes, it only provides an estimate of the overall material properties. Inspecting the anode block at different positions should provide more information about the distribution of pores and cracks within the volume, and provide a clearer diagnostic. This is essential for taking appropriate corrective actions on the anode manufacturing plant operation.

The objective of this work is to investigate the use of acoustic emission techniques for volumetric inspection of baked carbon anode blocks. It focuses on detection and identification of two types of internal voids, namely pores and cracks, using the attenuated acoustic signal propagating through the material. To prove the concept, a baked anode was sliced along its length and analyzed by CT-scan (X-ray) to reveal its internal structure [9]. Acoustic excitation waves at different frequencies were sent through the materials and the attenuated signals were measured at different positions from a certain number of slices. Several features were computed from the AE signals and collected in a data matrix which was then analyzed using Principal Component Analysis (PCA) [10]. The clustering patterns obtained in the PCA score space suggest that the proposed approach is sensitive to the concentration of pores and the size of cracks, and that both types of voids can be distinguished. The results were validated qualitatively using CT-scan images.

The paper is organized as follows. The experimental details about the acoustic emission set-up as well as the baked anode sample are presented first. The methods used for processing and analyzing the acoustic signals is described after which the results obtained with the proposed approach are discussed. Eventually, some conclusions are drawn.

2. Experimental

2.1. Acoustic emission system

An overview of the AE signal measurement system is shown in Figure 1. Signal conditioning was performed by pre-amplifiers. The conditioning signal (with a gain of 40 dB) was fed to the main data-acquisition board in which the AE waveforms and parameters were stored.

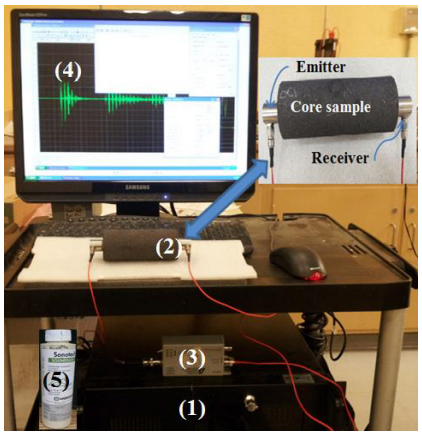

Figure 1. The acoustic system.

The system is composed of four Physical Acoustics™ (PAC) hardware components (MISTRAS Group Inc.). The components are identified directly within Figure 1 and are listed below:

(1) PAC SAMOS™ multi-channel acoustic emission system consisting of four 16-bit PCI-8 boards, including a 1-MHz AD converter on each channel.
(2) PAC R6-α AE resonant transducers (bandwidth 10k–1MHz, resonant frequency at 55 kHz, 15mm Ø).
(3) PAC model 2/4/6 pre-amplifier (10 kHz–2 MHz).
(4) PAC AE application software AEwin™ for SAMOS™.

Acoustic couplant (gel type) was also used to ensure a good contact between the AE sensors and the baked anode samples (number 5 in Figure 1). Note that an anode core sample is shown in this figure for illustration purpose only.

2.2. Baked anode samples

A full scale baked anode manufactured at the Alcoa Deschambault smelter located in Quebec, Canada (ADQ) was used in this work. The anode was first scanned using computed X-ray tomography (CT-scan) to reveal its internal structure [9]. Although this imaging technique is non-destructive in nature, it is it expensive to purchase and operate, and the scan is too time consuming to be used for routine anode inspection at the plant. Hence, the CT-scan images were used to qualitatively validate that the variations observed in the attenuated acoustic signals were associated with pores and cracks. The baked anode was sliced prior to imaging because the available instrument could not take samples as large as an anode. It was first cut into 26 slices of equal thickness along it length as shown in Figure 2 (left) and then each slice was cut further in halves along the height of the anode (see Figure 2 right). A total of 8 slices were selected for collecting the acoustic signals. These correspond to slice numbered 2, 3, 5, 7, 11, 15, 24, and 25 in Figure 2 (left). They were selected in such a way to obtain a representative sampling of the internal structure of the anode. Slices were selected at both ends of the anode as well as below and between the stub holes. It is well known in the field that spatial distribution of anode density, pore and crack concentration within the block is non-uniform, and that the internal structure at both ends of the anodes, below and between the stub holes are expected to be systematically different. Note that the top and bottom of each half slice were also cut prior to collecting the acoustic measurements to obtain samples of even height and standardize the sample geometry for all the selected slices (see Figure 2 right). Finally, each sample was divided into 6 corridors along the sample height as shown again in Figure 2 right. These corridors of equal width were drawn

using a white chalk. They were numbered 1 to 6 from the center of the anode toward its outer surface.

Figure 2. The sliced baked anode. Left: the selected 8 slices are identified in red. Right: example of a slices used for acoustic emission testing.

An example CT-scan result is shown in Figure 3 for slice number 7. The numbers within the image correspond to the 6 corridors drawn on the slices, in the same order as discussed previously (1 is at the center of the anode and 6 close to the outer surface). The image clearly shows the pores and cracks and regions of different densities (proportional to gray level intensities).

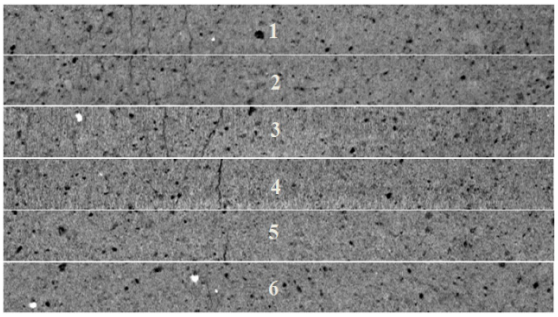

Figure 3. Example CT-scan image obtained for slice number 7.

2.3. Acoustic emission data collection

The AE sensors were mounted and put into close contact with the samples as shown in Figure 4. Both sensors (emitter and receiver) were positioned at both ends of a given corridor within a slice. They were maintained into position using a clamping device. The interfaces between the sensors and the material were filled with couplant gel in order to maintain appropriate signal transmission. The material in each corridor was then submitted sequentially to 7 different AE excitation frequencies (100, 130, 150, 170, 200, 230, and 250 kHz) while recording the attenuated acoustic signals. This procedure was repeated for each of the 6 corridors and for the 8 anode slices. In addition, preliminary work (not shown) has established that 250 kHz is the maximum excitation frequency for this material because the acoustic signal was found to be completed attenuated at higher frequencies. The data collection strategy was found to be repeatable and was not necessary to average several raw signals to reduce measurement errors. The sample surface

quality was similar for most samples. It is therefore considered that attenuation of the signal is mainly due to the material properties and voids (pores, cracks) and the effect of surface quality is negligible.

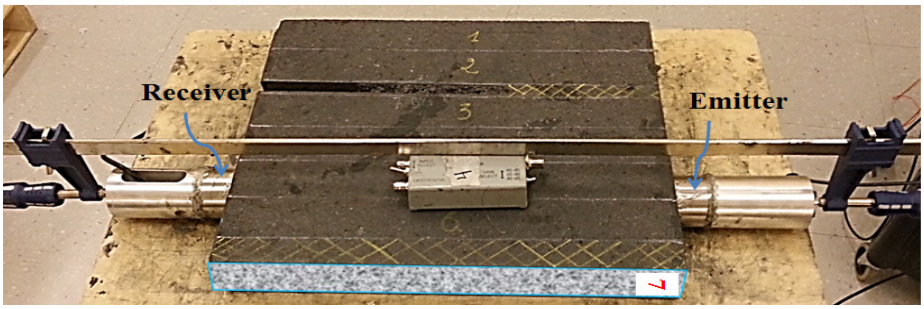

Figure 4. AE data acquisition set-up through different corridors of an anode slice.

Acoustic emission signals acquired at different frequencies on a particular corridor is shown in Figure 5 for illustration purpose. The signal attenuation pattern clearly changes as a function of the excitation frequency. According to acoustic emission theory, there is a relationship between the attenuation at a given frequency and the size of the voids inside a material. Higher frequency waves are attenuated by smaller voids compared to lower frequency waves. Hence, it is hoped that exciting the material at different frequencies should help detect variations in void sizes within the material.

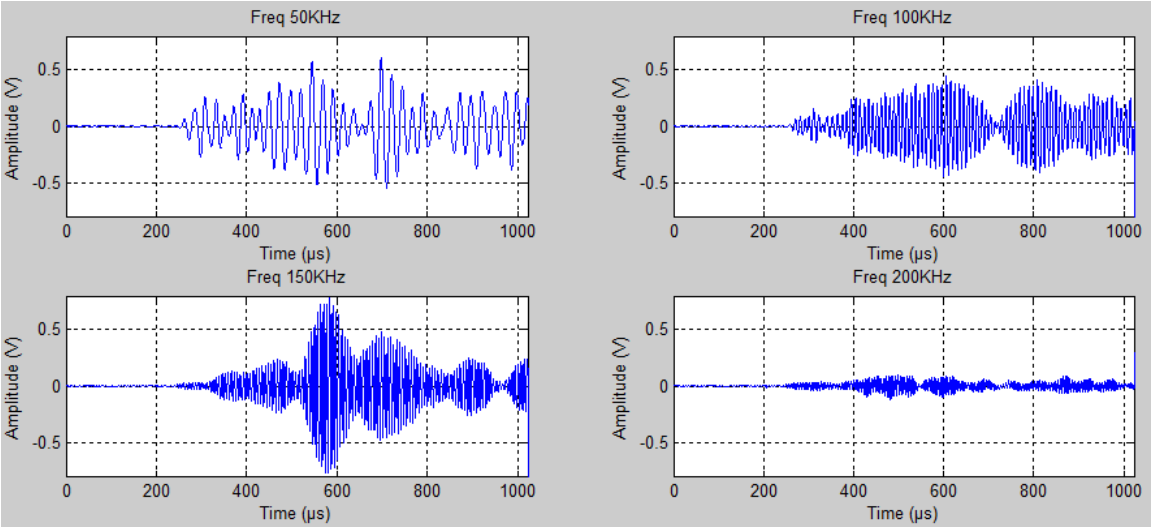

Figure 5. Examples of raw AE signals at acquired at different excitation frequencies.

3. Acoustic emission signal processing and analysis

3.1. Acoustic features extraction

Waveform processing of AE signals has routinely been used for detecting defects in materials. The acoustic wave propagating through the material attenuates at defects and discontinuities such as voids, cracks and inclusions. Hence, efficient techniques for AE signal analysis should allow distinguishing materials with and without defects. Although direct analysis of the entire raw AE signals could be performed using, for example, unsupervised clustering techniques such as

Principal Component Analysis (PCA) [11], it was rather decided to compute a small number of temporal features from each AE signal in order to reduce the size of the dataset to be analyzed. Indeed, a total of 7 AE signals were collected from the material contained in each corridor (one for each excitation frequency), and a raw AE signal is formed by several thousands of data points. A set of 7 time domain scalar attenuation features were therefore computed from each raw AE signal. These are the maximum, mean, standard deviation (STD), energy (E), root mean square (RMS), skewness (S) and kurtosis (K) of the AE signal time series x(i), i=1,2,…N :

$$MAX = \max_{i=1}^{N} x(i) \tag{1}$$

$$Mean = \bar{x} = \frac{1}{N}\sum_{i=1}^{N} x(i) \tag{2}$$

$$STD = \sqrt{\frac{1}{N}\sum_{i=1}^{N}(x(i)-\bar{x})^2} \tag{3}$$

$$E = \sum_{i=1}^{N}\left|x(i)\right|^2 \tag{4}$$

$$RMS = \sqrt{\frac{1}{N}\sum_{i=1}^{N}[x(i)]^2} \tag{5}$$

$$S = \frac{\frac{1}{N}\sum_{i=1}^{N}\left(x(i)-\bar{x}\right)^3}{STD^3} \tag{6}$$

$$K = \frac{\frac{1}{N}\sum_{i=1}^{N}\left(x(i)-\bar{x}\right)^4}{STD^4} \tag{7}$$

Where N is the total number of data points in the AE signal time series (same for all signals collected in this work). The above temporal features are commonly used in AE signal analysis [12]. Signal processing was performed using Matlab version R2014a (MathWorks, Natick, MA, USA).

The data was stored in a (48×49) dimensional matrix **X**. The 49 columns correspond to the 7 temporal features computed from the 7 AE signals collected from each of the 48 samples (6 corridors × 8 anode slices). Principal component analysis (PCA) was the used to analyze the information contained in the feature matrix **X**.

3.2. Principal component analysis (PCA)

PCA is a widely used multivariate statistical method for the analysis of large datasets containing noisy and highly collinear data, as is the case in this study. Assume a data matrix **X** (I×J) containing J measurements collected from I samples. Further assumed that both systematic variations and noise are present in this data. PCA decomposes the variance-covariance structure of **X** by finding a small number of orthogonal latent variables A <<< J capturing most of the systematic variations in **X**, but leaving noise or irrelevant information as residuals. These latent variables (also called components) are defined as linear combinations of the J original measurements and together define a lower dimensional subspace allowing easy visualization and interpretation of the information contained in large datasets. The PCA decomposition is expressed mathematically as shown below:

$$\mathbf{X} = \sum_{a=1}^{A} \mathbf{t}_a \mathbf{p}_a^T + \mathbf{E} \quad (9)$$

where the orthogonal vectors $\mathbf{t}_a$ (I×1) are those latent variables (called scores) providing the coordinates of each sample in the low dimensional subspace (plane or hyperplane) after projection. The subspace itself is defined by the A orthonormal loading vectors $\mathbf{p}_a$ (J×1), which are linear combinations of the original variables (i.e. $\mathbf{t}_a = \mathbf{X}\ \mathbf{p}_a$). The projection residuals are collected in the residual matrix **E** (I×J). The loading vectors are calculated in such a way that $\mathbf{t}_1$ explains the greatest amount of variance in **X**, $\mathbf{t}_2$ the second greatest amount of variance that not explained by the first component, and so on.

PCA effectively performs unsupervised clustering of the I samples in the latent variable subspace, which can be visualized using scatter plots of the scores (**t**'s). The differences between the clusters can be interpreted using the loading vectors (**p**'s). The reader is referred to Wold et al. [10] for more details about PCA. The ProMV software version 15.08 (ProSensus, Ancaster, ON, Canada) was used to build PCA models.

4. Results and discussion

The AE signals in a porous material, such as carbon anode material, usually have complex propagation characteristics. PCA was applied to the AE signal feature matrix **X** to assess whether the anode samples (corridors) located at different positions within the block could be distinguished based on their attenuation behavior (quantified by temporal features at different frequencies).

A total of 15 principal components (i.e. latent variables) were found statistically significant by a cross-validation procedure [13]. The cumulative sum of squares explained (R^2) and predicted (Q^2) by the first two PCA components are provided in Table 1. Only those two components are discussed since they were sufficient to discriminate the samples. They explain 65% of the variance in the attenuation features (**X**) while relatively good performance in prediction is maintained (Q^2=56%).

Table 1. Percent cumulative sum of squares explained (R^2) and predicted (Q^2) by the PCA model built on attenuation features collected from anode slices.

Component	R^2 (%)	Q^2 (%)
1	56,5	49,3
2	65,2	56,0

Figure 6 presents the latent variable score space for the two components of the model. Each marker corresponds to the attenuation behavior of one particular corridor (one row in **X**). Those were labelled in the plot using the slice and corridor numbers (slice#_corridor#) presented in Figure 2. The clustering pattern in the t_1-t_2 score space reveals that corridors 1-2, 3-5, and 6 of any slice cluster in 3 groups (black, orange and blue markers, respectively). At this point, it is important to remind that corridors #1 are located at the center of the anode and #6 at the outer surface. It can also be observed that the attenuation features of corridors 1-2 and 6 seem more variable than those of corridors 3-5 (orange cluster tighter than black and blue).

In order to interpret the differences between the three clusters based on the internal structure of the corridors, the CT-scan images of the 8 slices were examined first. In general, it was found that the central region of corridors 1-2 in most slices were showing several cracks, whereas the lower part of these corridors had a high density of pores. Corridors 3-5 were much denser with a few cracks, sometimes extending from corridors 1-2 in the transversal direction. Finally, corridors 6 rarely showed cracks but had a variable density of pores. Therefore, the clustering pattern shown in the score plot (Figure 7) suggests that the first component (t_1) is sensitive to the presence of cracks because from right to left in the score plot (along the t_1 direction), the corridors cluster according to the increasing presence of cracks. The second component, on the other hand, seems to distinguish dense from porous regions. Corridors 3-5 (orange markers) are denser and cluster in the negative t_2 region as opposed to those corridors characterized by a high pore density (most of corridors 1-2 and some 6) fall in the positive t_2 region. These results are also in agreement with carbon plant knowledge. The region below the stub holes corresponding to corridors 1-2 in slices #5, 7, 11, and 15 are generally expected to show a higher concentration of cracks. Most of these corridors fall in the cluster formed by the black markers. Corridors 1-2 in slices #24 and 25 (edge) project closer to the denser region (orange markers), which is normally expected unless cracks extend in the longitudinal direction from the center of the anode towards it surface as seems to be the case for the other edge of the anode (slices #2 and 3). Finally, it is important to understand that overlap between the clusters should not be interpreted as misclassification as it was not attempted to do so. Although cracks and pores are expected to concentrate in certain regions, they may very well be found in locations where they are less or not expected (hence the overlap between clusters) but still need to be detected by the AE inspection system. The color code used in Figure 7 was selected for illustration purpose only.

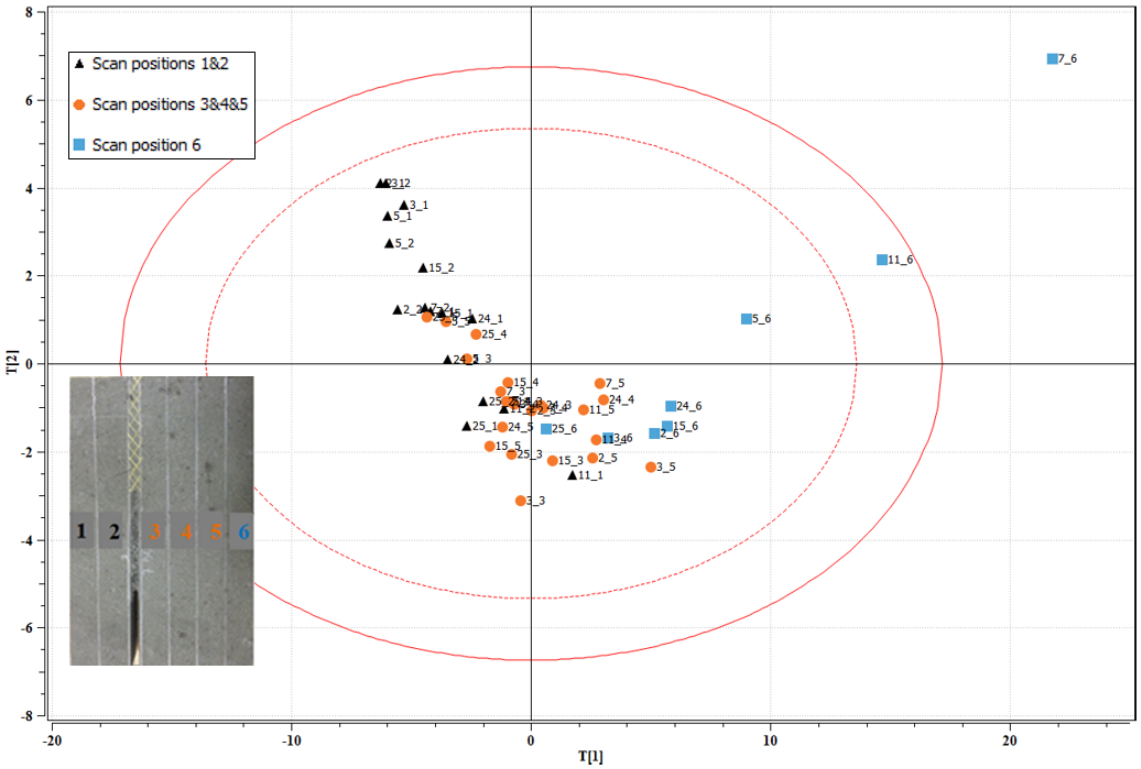

Figure 6. t_1-t_2 score plot of the PCA model built on AE signal attenuation features

The relationships between the clusters in the score space and the attenuation features is now discussed using the p_1-p_2 loading plot shown in Figure 7. As discussed previously, each score vector $\mathbf{t_a}$ is defined as a linear combination of the attenuation features (i.e. $\mathbf{t_a} = \mathbf{X}\,\mathbf{p_a}$), and the loading vector $\mathbf{p_a}$ contains the weights of each feature in that linear combination. The weights of each feature in both components are presented in the form of a scatter plot (Figure 7). Each point in this graph correspond to one feature calculated at one excitation frequency (i.e. one column of **X**). The labels are form by the feature name followed by the excitation frequency.

The loading plot is interpreted as follows. The absolute value of the loading weights indicate the important of the feature in a given component whereas the sign of the weights informs about the sign of the correlation between pairs of features. Those features having loading values of the same sign are positively correlated while those having positive signs are negatively correlated. Figure 7 reveals that the first component is mainly driven by the mean and the variance related features (max, E, RMS and STD). In addition, the mean features have an opposite sign compared to the others, indicating that it is negatively correlated with max, E, RMS, and STD. This means that moving from the positive t_1 region (low concentration of cracks) towards negative t_1 values (high concentration of cracks) involves lower values of the variance related features (max, E, RMS and STD) and higher values of the mean of the signal. This is consistent with AE signal attenuation by increasing concentration of cracks. The second component (orthogonal to the first) is mainly driven by features K and S which are negatively correlated at all frequencies, but at 200 kHz. In addition, their loading values switch signs around that frequency. This suggests that the presence of pores modifies the shape of the density distribution of the AE signal (as oppose to simple attenuation of the signal by cracks). Furthermore, the fact that the loading values for K and S are frequency dependent may indicate that t_2 is not only sensitive to pore concentration, but also their size. This is currently being investigated further.

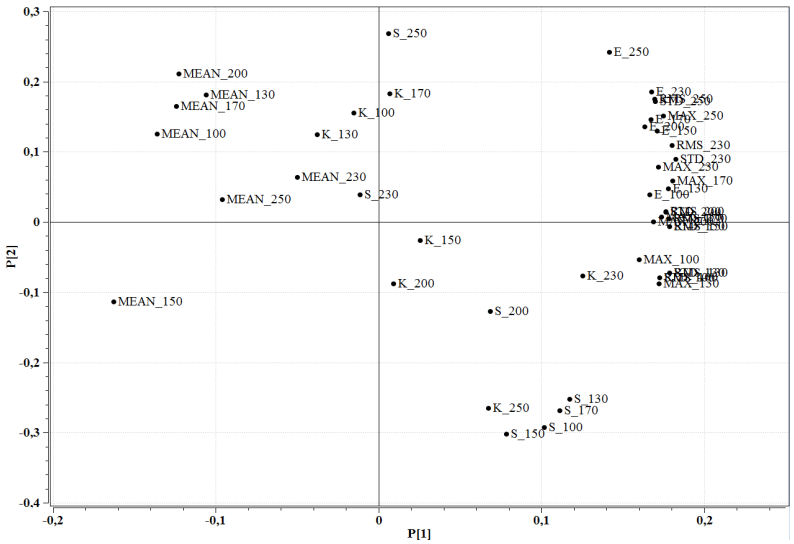

Figure 7. p_1-p_2 loading plot of the PCA model built on AE signal attenuation features

5. Conclusions

Acoustic emission (AE) was investigated as a potential rapid and non-destructive inspection technique for baked carbon anodes. A full scale anode was sliced in both longitudinal and transversal directions and imaged using CT-Scan (X-ray) to reveal its internal structure. AE

signal were then collected from several slices divided into corridors along the anode height. A vector of temporal attenuation features were calculated from each anode samples and then Principal component analysis (PCA) was applied to the attenuation feature matrix. The results have shown that the AE signal features are sensitive to the presence of cracks within the anode samples (measured by overall signal attenuation) and to the density of pores distributed throughout the block. The CT-scan images of the samples served as a reference for qualitative validation of the observations made from the AE signal features. The proposed approach appears very promising for full scale anode inspection. Future work should concentrate on validating the robustness of this method on several real anodes in plant to pave the way for the online control.

6. Acknowledgments

The research reported in this paper was funded by the Natural Sciences and Engineering Research Council of Canada (NSERC), by the Aluminum Research Center- REGAL, and by Alcoa Inc. This financial support is gratefully acknowledged. The assistance provided by REGAL personnel, Hugue Ferland and Guillaume Gauvin of Laval University, in preparing the experimental setup either in REGAL lab or in Alcoa Deshambault plant is also greatly acknowledged.

7. References

[1] Sinclair, K.A., and Sadler, B.A. Improving carbon plant operations through the better use of data, Light Metals 2006, pp 577–582.

[2] Sinclair, K.A., and Sadler, B.A. Which strategy to use when sampling anodes for coring and analysis. Start with how the data will be used, Light Metals 2009, pp 1037–1041.

[3] Kurz, J.H, Grosse, C.U., and Reinhardt, H.W. Strategies for reliable automatic onset time picking of acoustic emissions and of ultrasound signals in concrete, Ultrasonics. Vol. 43, (2005), pp. 538–546.

[4] Briche, G., Tessier-Doyen, N., Huger, M., and Chotard, T. Investigation of the damage behaviour of refractory model materials at high temperature by combined pulse echography and acoustic emission techniques, Journal of the European Ceramic Society. Vol. 28, (2008), pp. 2835–2843.

[5] Ohno, K., and Ohtsu, M. Crack classification in concrete based on acoustic emission, Construction and Building Materials. Vol. 24, (2010), pp. 2339–2346.

[6] Allaire, C. Methods and apparatus for non-destructive testing of materials using longitudinal compression waves, US patent number 5,040,419, Aug. 20 1991.

[7] Allaire, C., Allaire, J., and Carbonneau, A. Room and high temperature measurement of the elastic properties of refractories using a new apparatus and set-up, Light Metals 2004, pp. 629-636.

[8] http://www.d4m.com/soluss/cir/web/document/SonicByte-Presentation.pdf (last access September 2nd 2015).

[9] Picard, D., Lauzon-Gauthier, J., Duchesne, C., Alamdari, H., Fafard, M., and Ziegler, D. Automated crack detection method applied to CT images of baked carbon anode. Light Metals 2014, pp. 1275-1280.

[10] Wold, S., Esbensen, K., and Geladi, P. Principal Component Analysis, Chemometrics and Intelligent Laboratory Systems. Vol. 2, (1987), pp. 37-52.

[11] Johnson, M. Waveform based clustering and classification of AE transients in composite laminates using principal component analysis, NDT & E International. Vol. 35, (2002), pp. 367-376.

[12] Miller, R.K., and McIntire, P. Nondestructive testing Handbook – Acoustic Emission Testing, American Society for Nondestructive Testing (1987), p. 30, ISBN [13] 9780931403026.

[13] Wold, S. Cross-validatory estimation of the number of components in factor and principal component models, Technometrics. Vol. 20, (1978), pp. 397-405.